Carrier Differential GPS for Real-Time Control of Large Flexible Structures

E. Harrison Teague, Jonathan P. How, Bradford W. Parkinson

Department of Aeronautics and Astronautics, Stanford University

BIOGRAPHY

E. Harrison Teague is a Ph.D. candidate in Aeronautics and Astronautics at Stanford University. He received his B.S. in Aerospace Engineering from Virginia Tech in 1991, and his M.S. from Stanford in 1993. He has worked on GPS receiver design at Trimble Navigation, Ltd. in Sunnyvale, CA.

Jonathan P. How, Ph.D., is an Assistant Professor in the Department of Aeronautics and Astronautics at Stanford University. He received his B.A.Sc (1987) from the University of Toronto, and his SM (1990) and Ph.D. (1993) from MIT both in Aeronautical and Astronautical Engineering.

Bradford W. Parkinson, Ph.D., is a professor of Aeronautics and Astronautics at Stanford University, and Program Manager of the Relativity Gyroscope Experiment (Gravity Probe B). He served for six years as the first Program Director of the GPS Joint Program Office, and has been instrumental in GPS program development. Dr. Parkinson heads the NASA Advisory Council and is on the Vice President's Committee on Aviation Safety and Security. He is a Fellow of the AIAA and a member of the National Academy of Engineering.

ABSTRACT

Current lab tests demonstrate vibration and orientation control of highly flexible vehicles using only the GPS carrier to measure motion. A 30-foot long test structure has been constructed that is suspended from above, and moves in an analogous way to a flexible orbiting platform. The test structure is outfitted with an array of GPS antennas for motion sensing, and an array of compressed air thrusters for control actuation. The sensor has shown better than 0.5 degree rotational accuracies as measured with respect to on board rate gyroscopes. We have shown simultaneous rigid-body orientation and elastic vibration control by closing a feedback loop from the GPS differential carrier phase (DCP) measurements to the thruster commands.

Central to the success of the GPS deformation sensing system is the sub-centimeter level differential position information available from GPS carrier tracking. However, it is challenging to use this accuracy due to inherent, and arbitrarily large, measurement biases. Bias resolution (akin to cycle ambiguity resolution) has been solved for vehicle navigation and attitude determination problems. We show bias estimation for an antenna array mounted on a structure whos relative antenna motions due to flexibility are on the same order of magnitude as those due to overall attitude changes.

This research is a significant step toward general distributed antenna array GPS carrier based sensing systems. Our techniques are applicable to systems that exhibit relative motions with frequencies (< 10 Hz) and deflections (> 1 cm) that are detectable by current receivers.

Presented at ION-GPS96, Kansas City, Missouri, September 17-20, 1996.

1 INTRODUCTION

The widespread availability of the GPS signal is having a revolutionary effect on positioning and naviga-

Figure 1: Experimental structure in motion

tion. In particular, the ability to obtain centimeter level position information by tracking the GPS carrier has opened up a wide range of applications, from terminal navigation of aircraft [3], to automatic control of farm and construction vehicles [9], to guidance and control of spacecraft [2]. The difficulties in using carrier information, such as cycle ambiguity and timing errors, have been the subject of intense research in the recent past.

The majority of carrier based sensing systems rely on differencing carrier measurements between pairs of antennas in an antenna array. The antenna motions may be highly correlated, such as in rigid body attitude determination [4], or uncorrelated, such as in free-flying space robot navigation [13]. The focus of this research is to extend the use of differential carrier phase (DCP) tracking to the case where antenna motion is consistent with flexible body dynamics. Cohen shows the measurement of aircraft wing flexure in an attitude sensor in [4]. In our previous work, these ideas are generalized to measurement of structural flexibility for systems whose antenna motion is dominated by structure deformations. Simulations and filter design are presented in [12], and spectral analysis verifying the modal observability for our experimental system is shown in studied in [11].

In this paper, techniques of using a system model for initial and real-time data processing are shown, and the experimental verification of these ideas is presented. This research is unique in that it shows real-time control of a system with complicated elastic and rigid-body dynamics, using only the DCP measurements from a distributed array of antennas as the motion sensor. A picture of the experimental apparatus is shown in Fig. 1.

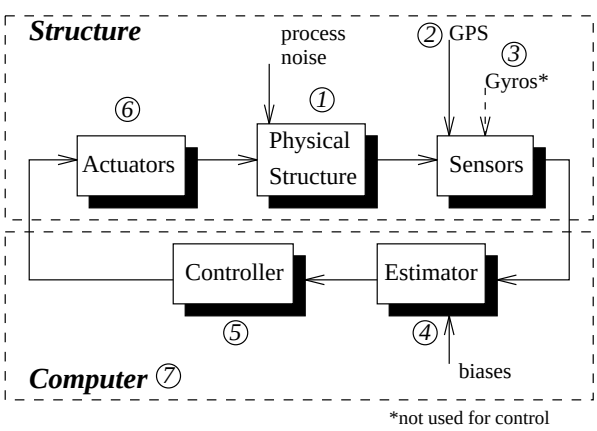

Figure 2: Elements in the Control Loop

2 THE GPS/FLEXIBLE STRUCTURE EXPERIMENT

2.1 Experimental Objectives

The following is a list of our experimental objectives:

1. Design an estimator that can observe selected rigid-body and elastic deformation states in real-time using only GPS measurements.
2. Evaluate the accuracy of the state estimates by comparing them with estimates based on independent rate gyro measurements.
3. Successfully damp elastic vibrations in the test structure with a real-time control system.
4. Demonstrate an automatic rigid-body orientation slew maneuver with simultaneous structural vibration control.

2.2 Experimental Setup

A diagram of the main elements of the experimental setup and their interconnection is shown in Fig. 2. The numbers in the following list correspond to the numbered labels in the figure. The hardware descriptions here are brief; see [11] for more details.

1. The physical structure.

The structure is an aluminum body that hangs from twelve meter threads from an overhead crane in our laboratory. A diagram of the structure is shown in Fig. 3. The structure consists of three massive rigid bodies (65 kg) that are connected together by long, elastic aluminum tubes in a horizontal line. This configuration was selected to achieve relatively large, low frequency deflections in the lab environment. The tubes provide enough elasticity to allow the whole structure to vibrate slowly with significant deflections. Passive structural damping is very small (time constants of several minutes), making the system suitable for active vibration control.

The suspension threads are attached at the top to a rigid beam that is mounted to a bearing, allowing the beam, and the structure below, to rotate freely in the horizontal plane. The system provides a platform whose motions will be detectable by GPS antennas mounted on the structure.

The estimator and controller make use of a dynamic model of the test structure that was computed using MSC/NASTRAN on the Cray computer at NASA

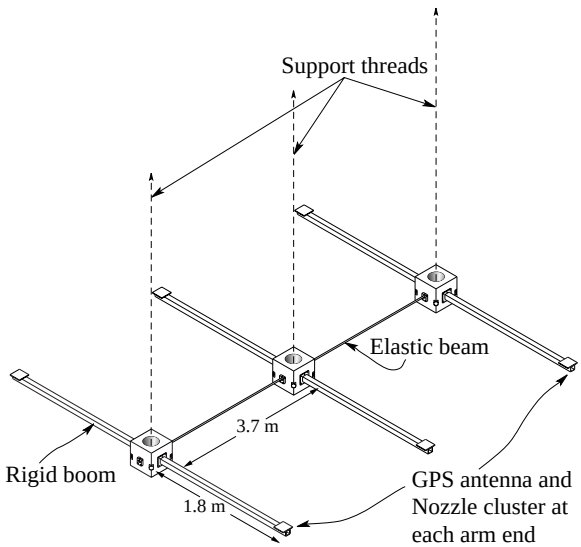

Figure 3: The test structure

Ames. Suspension induced modes were predicted in addition to the structure's elastic modes. The modal frequencies predicted by this model were adjusted to better fit Fourier transformed experimental data. The final linear model contains under 10 modes below 2 Hz.

2. The GPS sensors.

Since the testing is done indoors, the signals from the GPS satellites are not detectable. Therefore, a set of six pseudolite transmitters were constructed and mounted on the ceiling and walls of the laboratory. The transmitters are equally distributed in the "sky" to provide favorable signal geometry. One of the pseudolites was modified to broadcast a data message that is used for coarse synchronization of our GPS receivers.

Two hemispherical GPS patch antennas are mounted to each rigid body for a total of six antennas (a seventh antenna is also on a static stand in the lab, and was used for calibration and testing, but is not essential to system operation). Two 4-antenna Trimble TANS Quadrex© receivers measure the pseudolite signals and output DCP measurements at 10 Hz. The receiver core code is modified at the signal processing level to suit the experiment requirements. The signal from one of the antennas on the structure is split and runs to both receivers. This common signal at each receiver allows carrier measurements to be differenced only between antennas connected to the same receiver, which eliminates timing errors (see Appendix A).

The resulting GPS sensing system consists of an array of interconnected antennas that provide enough information to resolve the overall motion with sufficient bandwidth and deflection sensitivity for control. The DCP measurement equation is discussed further in Section 3.

3. The rate gyros.

Six inexpensive rate gyroscopes were mounted to the test structure primarily to provide an independent measurement with which to compare the GPS results. It is possible to take advantage of the good high frequency performance of the gyros to enhance state estimates [8], although this is not currently being done.

4. State Estimator

The states of the experimental system are defined as selected elastic and rigid-body structural modes, and their derivatives. These states are estimated in real-time using an extended Kalman Filter that has been optimized for execution speed. The original analytical filter development for this work is shown in [12]. The time updates of the filter are computed using the NASTRAN dynamic model.

The measurement updates are computed from the measurement equation linearized about the current estimated state. Relinearization is performed only when the state perturbations from the previous linearization exceed certain thresholds, minimizing unnecessary processing.

The measurement equation and its gradients are formulated using the symbolic manipulator, Autolev©, to process the vector functions of the state variables. A custom text file manipulation code was written in Perl that reads the Autolev output, and generates a C language program that can then be compiled and linked with the real-time application. The automatically generated C code text file is over 100 kilobytes in size, but executes in less that 5 milliseconds on a Pentium© 200.

The state estimator relies on an initialization process that provides an estimate of the biases intrinsic to DCP measurements. Bias estimation is discussed further in Section 4.

Experimental results of the estimator are shown and discussed in Section 2.4.

5. Controller

The controller used for the data presented in this paper is a multi-input multi-output full-state regulator that minimizes a quadratic function of weighted states and control outputs (known as a linear quadratic regulator, or LQR). The weights were set initially from our estimates of noise magnitude, and finally tuned by processing simulated data. Further control design

may improve real-time performance, and is a topic for further investigation.

6. Actuators

A system of 24 on/off cold gas thrusters is used to impart forces on the test structure. The system pressure is 100 psi and each thruster can deliver ~ 2 Newtons of force. The thruster positions and orientations were chosen to provide controllability of all modes of interest, while minimizing the number of thrusters. The thruster valves are capable of cycling at a maximum rate of 100 Hz.

Continuous control force requests from the controller were realized using pulse - width, pulse - frequency (PWPF) modulation of the on/off valves.

7. Real-time computer

Real-time data collection, processing and control implementation were performed on a Pentium Pro 200 running LynxOS© Ver. 2.4.0 from Lynx Real-Time Systems© [7]. The code was written in a multithreaded, priority based framework conforming to POSIX real-time standards.

2.3 Real-Time Data Processing

Fig. 4 illustrates the main components of the real-time code. GPS data is received though two serial ports, and stored in global space. When the state estimator is signaled of the presence of new data, it processes the data and control feedback is computed based on the new estimates. This control feedback is passed to the control modulator that commands the thruster valves though a digital I/O card.

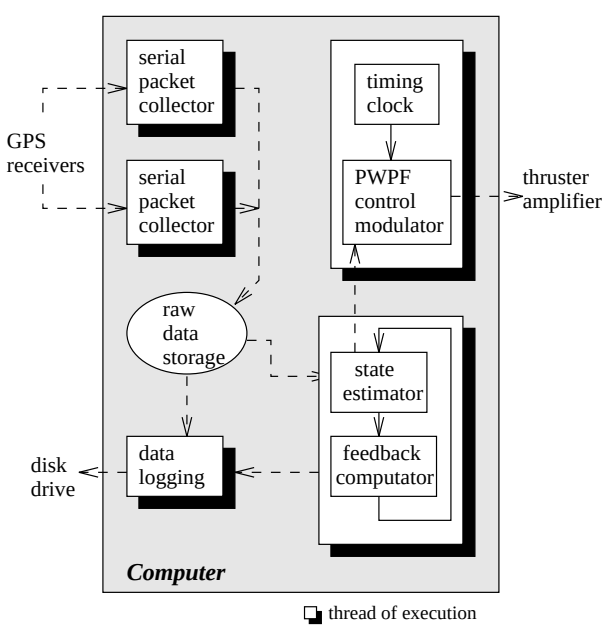

Figure 4: Real-Time Processing Setup

2.4 Real-Time Estimator Results

Fig. 5 plots estimates of the rotation angle of the structure's center rigid body about a lab fixed vertical axis. This data was processed in real-time subsequent to a dynamic bias estimation (see Sec. 4.3). The structure is initially rotated (manually) as a whole in the horizontal plane to illustrate state estimation during a large scale platform slew. Then (at about 140 seconds), the structure is randomly excited to illustrate estimation during elastic vibration.

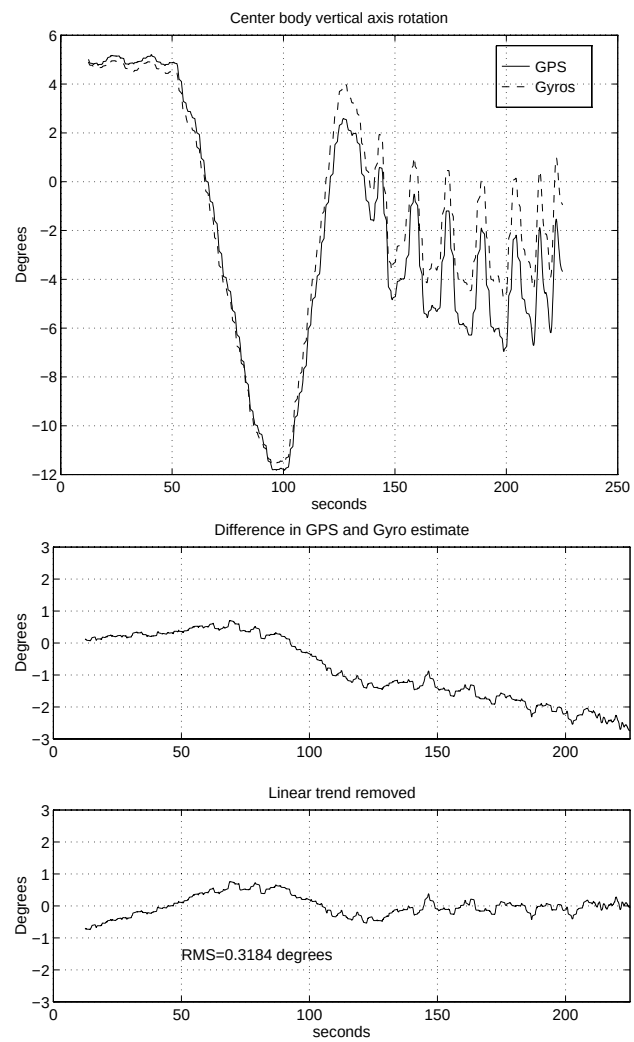

Figure 5: Comparison of GPS and Gyro based estimates.

GPS based and gyro based estimates are plotted. The gyro estimate is obtained by integrating the body fixed vertical axis gyro signal, which is equal to the laboratory fixed rotation for small out-of-plane rotations. The second plot shows the difference between the two estimates. The first and the second figure show a linear trend in the difference that is attributable to drift in our gyroscopes. The third plot shows the difference with the linear trend removed. For analysis of GPS estimates, it is fair to remove this trend which is known to be contributed by the gyros alone. The third plot shows that the difference is always less than one degree, and has an RMS value of 0.3 degrees. These results show that the estimates based on the independent sensors agree during both the slew maneuver and during elastic vibration.

These results are significant in that they show a sub-degree, sub-centimeter sensor of general structural deformations with zero drift characteristics. This performance is available wherever the GPS signal environment exists, or can be re-created (such as in our laboratory).

2.5 Real-Time Control Results

Thus far, we have discussed our GPS sensor system and estimation objectives. Now we present experimental test results that address our goals for real-time control. The first test illustrates active vibration damping. The structure was perturbed manually such that it vibrated "randomly" with relative antenna deflections on the order of 10 to 20 centimeters. Due to the low system damping, vibrations typically persist for 5 to 10 minutes after excitation. Fig. 6 shows estimated angles of rotation of each of the three rigid sections about the longitudinal twist axis (coincides with the elastic beams when the structure is at rest, see Fig. 3) during this vibration. The first 15 seconds show free motion. At about 15.5 seconds on the plot, the control loop is closed, and the thrusters begin firing. Vibration damping is achieved with a settling time of ~ 5 seconds, and the angles are controlled to within *0.15 degrees* as measured by GPS.

The second plot in Fig. 6 shows two raw integrated gyro measurements. In contrast with the top plot of estimator outputs, this shows unfiltered structure motion measurements before and after loop closure. The bottom plot of Fig. 6 shows the difference between the GPS and Gyro based state estimates.

The next experiment was a test of the feedback system's ability to perform a slew maneuver. The structure was rotated 16° in the horizontal plane and left

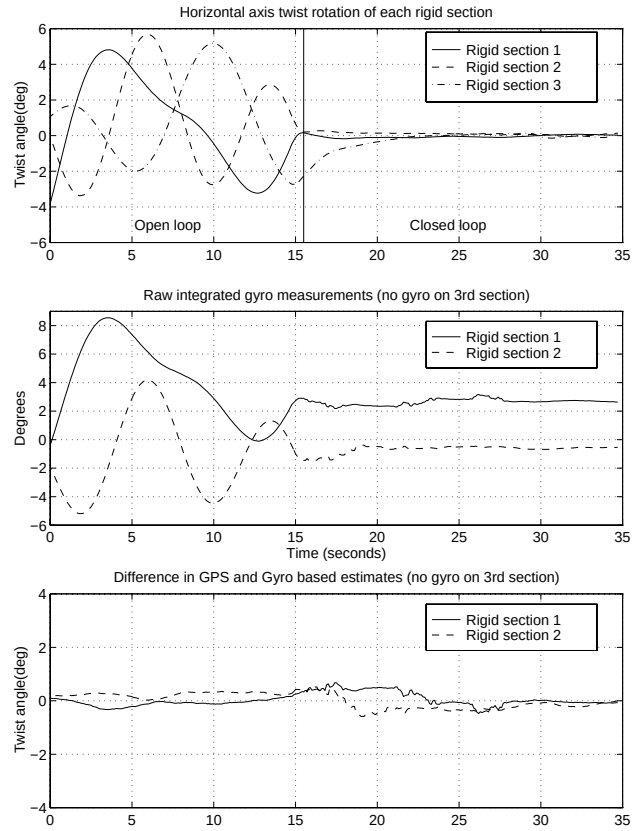

Figure 6: Elastic vibration control

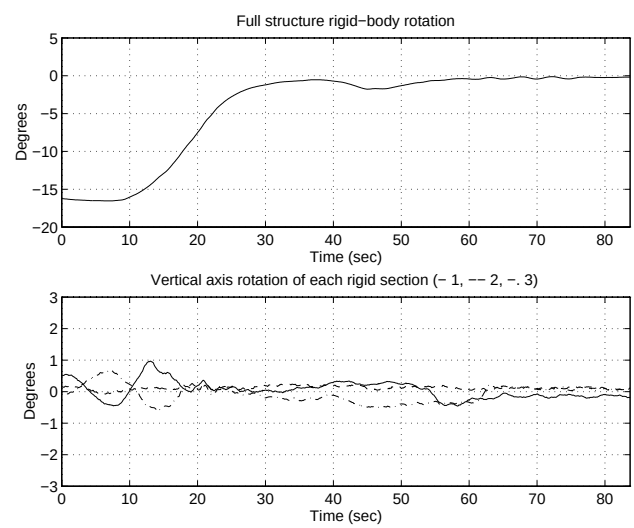

Figure 7: Slew maneuver control

at rest. At time zero, a command for 0° rigid-body angle was issued to the control system. The maneuver settled within thirty seconds, which is fast given the limited thruster force and large rotational inertia associated with this motion. Fig. 7 shows the time response plots. The first plot is the estimated slew angle,

which settles to within a half of a degree as measured by GPS. The second plot shows the relative vertical axis rotations of each of the rigid sections of the structure. These plots indicate the ability of the control system to simultaneously regulate internal vibrations (to within a degree) during a slew maneuver.

The experimental results given in this paper depend on the ability to make sub-centimeter level GPS carrier based relative position measurements, and the ability to resolve a system's states given these measurements. The following two sections discuss the basics of DCP and some methods for resolving the bias unknowns associated with these measurements.

3 DCP MEASUREMENT EQUATION

This research uses carrier measurements that are differenced relative to a common clock reference. This is achieved by multiplexing several antennas connected to the same receiver. (The general carrier phase observable is developed in Appendix A.) The resulting DCP measurement equation is illustrated in Fig. 8. In our current receivers, a DCP measurement is the difference in phase at a "master" antenna and one of the "slave" antennas. The vector between the antennas is called the "baseline vector." The measurement consists of the difference in the line-of-sight distance from a transmitter to each antenna, plus a bias that is fixed at the time of carrier lock at each antenna. In some cases, this bias may be written as the sum of the so called integer ambiguity and line bias, but for this paper, the quantity is left as a general bias.

$$\Delta\phi_{ij} = |\underline{p}^{N_j P_i}| - |\underline{p}^{N_j P_M}| + b_{ij} + \nu_{ij} \tag{1}$$

where,

- $\Delta\phi_{ij}$ - DCP of baseline i, transmitter j
- P_i - the point corresponding to the phase center of antenna i ($i = M$ denotes the master antenna)
- N_j - the point corresponding to the phase center of transmit antenna j
- $\underline{p}^{N_j P_i}$ - position vector from N_j to P_i
- b_{ij} - the bias associated with baseline i and transmit antenna j
- ν_{ij} - stochastic noise

If the transmitter is sufficiently distant from the antennas, the received wavefront is well approximated as planar. This allows the carrier phase measurement to be written as vector dot product of the baseline vector with the line-of-sight vector to the transmitter. Our indoor experiment uses pseudolite transmitters that are too close to the experiment to allow for the planar assumption. See [11] for further details.

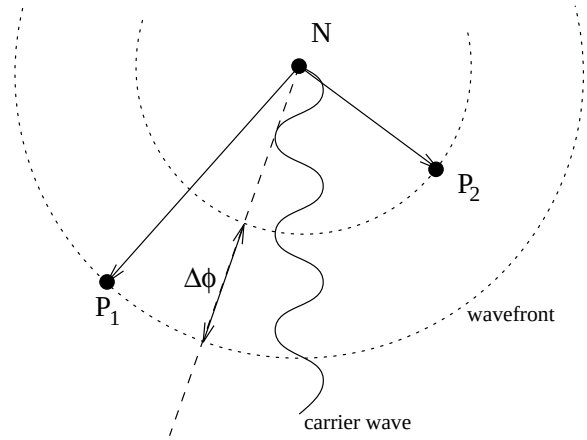

Figure 8: DCP Measurement

The next step is to form the vector measurement equation for the whole system by stacking measurements.

$$\Delta\phi \underset{(1)}{=} h(x) + b + \nu \tag{2}$$

Unsubscripted symbols denote a vector of stacked quantities, and x represents the system state. (A number under the equals sign is a reference to a previous equation). $h(x)$ contains the geometric functional dependence in the measurements, and depends on the vector magnitudes, which in turn depend on x[1].

We may linearize (2) about a nominal state, $\bar{x}$ to form,

$$\Delta\phi \underset{(1)}{\cong} H(\bar{x})\delta x + h(\bar{x}) + b + \nu \tag{3}$$

where,

$$x = \bar{x} + \delta x$$
$$H(\bar{x}) = \left.\frac{\partial h}{\partial x}\right|_{x=\bar{x}} \tag{4}$$

Since there are always as many unknown biases as measurements, this system of equations is underdetermined. Hence, another method of estimating b is sought.

4 BIAS ESTIMATION

The purpose of a bias estimator is to find b in Eq. (2). Three types of estimators (in order of increasing com-

[1] For non-planar wavefronts, $h(x)$ also depends strongly on the transmitter phase center locations, which must be estimated. An algorithm based on GPS measurements was developed for our experimental work and used for this task, but is not presented here.

plexity) will be discussed: static, kinematic, and dynamic.

First, we simply show the formulation of the mathematics of each estimator type. Then, in Section 4.4, we discuss the operational differences in the estimators and state how each estimator was used, and how it performed, in our experimental work.

4.1 Static

A static bias estimator is simple, but is rarely practical for operational use because it requires motionless data collection during which an accurate state estimate is known. The biases then may be computed from (2) as $\hat{b} = \overline{\Delta\phi} - h(\hat{x})$, where $\overline{\Delta\phi}$ is the averaged phase measurements and $\hat{x}$ is the best guess of the state. If $\Delta\phi$ is zero mean, the primary source of bias error is errors in the state estimate, $\hat{x}$. The sensitivity of $\hat{b}$ may be analyzed by computing the maximum singular value of $H(\hat{x})$ from (4). This gives an indication of the potential worst case bias error due to small errors in $\hat{x}$.

4.2 Kinematic

A kinematic bias estimator uses multiple measurement sets (the ith set being a vector of measurements taken from the system that is in some state, $x^{(i)}$), and uses the knowledge that the biases are constant, to form an overdetermined system. If there are n states and m measurements per set, combining N sets and linearizing yields,

$$\begin{bmatrix} \delta y^{(1)} \\ \delta y^{(2)} \\ \vdots \\ \delta y^{(N)} \end{bmatrix} \underset{(3)}{=} \left[\begin{array}{cccc|c} H^{(1)} & & & 0 & I \\ & H^{(2)} & & & I \\ & & \ddots & & \vdots \\ 0 & & & H^{(N)} & I \end{array}\right] \begin{bmatrix} \delta x^{(1)} \\ \delta x^{(2)} \\ \vdots \\ \delta x^{(N)} \\ \delta b \end{bmatrix} + \nu \tag{5}$$

$$\text{or,} \qquad \delta y \underset{(5)}{=} \tilde{H} \begin{bmatrix} \delta x \\ \delta b \end{bmatrix} + \nu \tag{6}$$

where the superscript is the measurement set index and,

$$\delta y^{(i)} = \Delta\phi^{(i)} - h(\bar{x}^{(i)}) - b \tag{7}$$

$$H^{(i)} = H(\bar{x}^{(i)}) \tag{8}$$

$\delta y^{(i)}$ is the measurement residual. If the system is observable, a solution may be found by iterating the weighted least-squares equation with weights defined by the diagonal matrix, R (a good choice of R is an estimate of the inverse of the measurement noise covariance),

$$\begin{bmatrix} \delta\hat{x} \\ \delta\hat{b} \end{bmatrix} = \left(\tilde{H}^T R \tilde{H}\right)^{-1} \tilde{H}^T R \delta y \tag{9}$$

For this system to be observable, $\tilde{H}$ must have full column rank. First, this requires that you collect enough data sets such that $\tilde{H}$ is "tall." This requires $N > \frac{m}{m-n}$. Another interesting requirement for observability is that no column of $H^{(i)}$ be constant for all i (see Appendix B for proof). This indicates that the measurement, $h(x)$, must be a non-linear function of the state x, and that data, δy, must depend on this nonlinearity. Further, the sensitivity of *each* state variable (column of $H^{(i)}$) must be a function x.

These observations lead to somewhat detailed requirements for system motion during data collection. An alternative that may provide a better bias estimate, given a sufficiently accurate model, uses knowledge of system dynamics.

4.3 Dynamic

If the antennas are mounted to a system for which we have a dynamic model, it is possible to use this information to improve our bias estimate. For example, say we are given a (discrete) dynamic model of the form,

$$x_{i+1} = Ax_i + Bw_i, \quad i = 1, ...N \tag{10}$$

If we form the augmented state as,

$$x_{aug} = \begin{bmatrix} b \\ x_1 \\ w \end{bmatrix} = \begin{bmatrix} b \\ x_1 \\ w_1 \\ w_2 \\ \vdots \\ w_{N-1} \end{bmatrix} \tag{11}$$

a linearized equation that incorporates all the data and known system information is given by Eq. (12) [1] (on next page).

The procedure for performing a batch dynamic solution of the measurement biases is as follows.

1. Collect and store N sets of data equally spaced data as the physical system is in motion.
2. Define the diagonal weighting matrix $W^{-1} = E[w_i w_i^T]$ as the best estimate of the process noise covariance. As in Eq. (9), define $R^{-1} = E[\nu_i \nu_i^T]$ as the best estimate of the measurement noise covariance.

$$
\begin{bmatrix} \delta y^{(1)} \\ \delta y^{(2)} \\ \vdots \\ \delta y^{(N)} \\ \hline 0 \\ 0 \\ \vdots \\ 0 \end{bmatrix}
=
\left[\begin{array}{cccccc}
I & H^{(1)} & 0 & 0 & & 0 \\
I & H^{(2)}A & H^{(2)}B & 0 & & 0 \\
I & H^{(3)}A^2 & H^{(3)}AB & H^{(3)}B & \cdots & 0 \\
I & H^{(4)}A^3 & H^{(4)}A^2B & H^{(4)}AB & & 0 \\
 & & \vdots & & \ddots & \vdots \\
I & H^{(N)}A^{N-1} & H^{(N)}A^{N-2}B & H^{(N)}A^{N-3}B & \cdots & H^{(N)}B \\
\hline
 & & & I & & \\
\end{array}\right]
\begin{bmatrix} \delta b \\ \delta x_1 \\ \delta w_1 \\ \delta w_2 \\ \vdots \\ \delta w_{N-1} \end{bmatrix} + \nu \tag{12}
$$

or,

$$
\left[\frac{\delta y}{0}\right] \underset{(12)}{=} \left[\frac{C}{I}\right] \begin{bmatrix} \delta b \\ \delta x_1 \\ \delta w \end{bmatrix} + \nu \tag{13}
$$

3. Define the diagonal weighting matrices, β and X_1. These determine the relative weighting of the b and x_1 portions of the state. They may be set to zero, or scaled to improve convergence of the batch estimator.

4. Perform the batch solution by iterating Eq. (14) until convergence.

$$
\begin{bmatrix} \widehat{\delta b} \\ \widehat{\delta x_1} \\ \widehat{\delta w} \end{bmatrix} = \left(C^T R C + \begin{bmatrix} \beta & & \\ & X_1 & \\ & & W \end{bmatrix} \right)^{-1} C^T R \delta y \tag{14}
$$

4.4 Discussion of Bias Estimators

The static estimator may have value for certain cases due to its computational simplicity. Given a static bias estimate based on a state guess, $\hat{x}$, subsequent (kinematic least-squares) state estimate errors are equal to the error in $\hat{x}$, as long as the linearization in (3) remains valid. However, most applications do not satisfy this property.

Kinematic algorithms have been used exclusively for the research on which this work builds [4, 9, 10]. Their advantage is speed and simplicity. The sparse structure of Eq. (5) can be exploited for efficient computation. However, we have not yet obtained usable bias estimates from a kinematic algorithm due to insufficient observability in our experimental system.

It is possible to refine bias estimates using the additional information in a system model. Using a known correlation between states over time, and a known statistical character of process noise, bias observability and estimate accuracy can be improved. A dynamic approach has not been used for previous projects because a model did not exist which was accurate enough to add information to the high-precision GPS carrier measurements.

The best bias estimator for a particular application depends on several factors, including model accuracy, required estimate accuracy, and motion available during data collection. All of the experimental results presented in this paper used the dynamic algorithm in Sec. 4.3.

Finally, the bias estimators presented here use a batch approach, where the estimate update is computed using all the available data simultaneously. It is possible to use iterative recursive smoothing techniques to arrive at the same result [5]. The computational efficiency of recursive processing is superior, especially for systems with many states. Also, recursive techniques are more flexible to operational non-idealities, such as temporary signal losses, etc. [10]. However, a much better initial guess is needed for the recursive than the batch algorithm for reliable convergence. Due to this limitation, we chose a batch algorithm for our experimental work.

5 CONCLUSIONS

The experimental results presented in this paper are promising for a number of reasons:

1. Estimation of the elastic and orientation states of a highly flexible structure was shown using *only* GPS carrier measurements. Rotation estimate accuracies of 0.3 degree standard deviation were measured relative to independent gyro sensors.

2. The implication is that high accuracy, zero-drift deformation measurements are available anywhere the GPS signal environment exists, or can be created.

3. A constant gain controller based on a simple linear dynamic model was able to control both structural orientation and elastic vibrations simultaneously using pulsed thrusters for actuation. Tests show vibration settling times on the order of 10 seconds, to sub-centimeter/sub-degree positioning accuracy.

4. These results show the use of GPS for control of a system with complicated dynamics depending on many parameters (our experiments use 36 measurements and 18 states). This represents a next step in sophistication of distributed antenna GPS sensing systems.

Three different methods of resolving the intrinsic bias uncertainty in DCP measurements are shown. The appropriate method for an application depends on requirements for simplicity, accuracy, and reliability.

We believe that this system is directly applicable to real systems which have motions in the bandwidth and sensitivity limits of current receiver technology. The only requirement is the existence of a GPS signal environment, which could be supplied by the GPS satellites, by pseudolites, or both. Further system performance could be obtained by more accurate model determination (either analytically, or by using measurement based system identification), and more refined control compensator design.

6 ACKNOWLEDGMENTS

We would like to thank several individuals and organizations whose participation in this research has been invaluable. We acknowledge London Lawson for the design and constructed the actuation system. Thanks to Michael Boerjes for the hardware interface to the sensors and actuators. Thanks also to Kurt Zimmerman, Konstantin Gromov, Stewart Cobb, Paul Montgomery and Clark Cohen for valuable help and suggestions.

We gratefully acknowledge Trimble Navigation for providing receivers and access to the receiver's core source code. This research is funded by NASA contract NAS8-39225.

References

[1] Arthur E. Bryson. Class Notes, Optimal Estimation with Uncertainty. Stanford University, 1993.

[2] C. E. Cohen, E. G. Lightsey, B. W. Parkinson, and W. A. Feess. Space Flight Tests of Attitude Determination Using GPS. In *Proceedings of the Institute of Navigation GPS-93 Conference*, Salt Lake City UT, 1993.

[3] Clark Cohen, David Lawrence, Boris Pervan, H.Stewart Cobb, Andrew Barrows, David Powell, Bradford W. Parkinson, Victor Wullschleger, and S. Kalinowski. Flight Test Results of Autocoupled Approaches using GPS and Integrity Beacons. In *Proceedings of the Institute of Navigation GPS-94 Conference*, Salt Lake City UT, 1994.

[4] Clark Emerson Cohen. *Attitude Determination Using GPS.* PhD thesis, Stanford University, Department of Aeronautics and Astronautics, Stanford, CA 94305, December 1992.

[5] Arthur Gelb. *Applied Optimal Estimation.* MIT Press, Cambridge, MA, 1974.

[6] Thomas Kailath. *Linear Systems.* Prentice-Hall Information and System Sciences Series. Prentice-Hall, Englewood Cliffs, NJ, 1980.

[7] Lynx Real-Time Systems, 2239 Samaritan Drive, San Jose, CA 95124. *LynxOS 2.4.0 Users Manuals*, 1995.

[8] Paul Y. Montgomery, H. Uematsu, and B. W. Parkinson. Analysis of Angular Velocity Determination Using GPS. In *Proceedings of the Institute of Navigation GPS-94 Conference*, Salt Lake City UT, 1994.

[9] Michael L. O'Connor, Gabriel H. Elkaim, and Bradford W. Parkinson. Kinematic GPS for Closed Loop Control of Farm and Construction Vehicles. In *Proceedings of the Institute of Navigation GPS-95 Conference*, Palm Springs CA, September 1995.

[10] Boris Steven Pervan. *Navigation Integrity for Aircraft Precision Landing Using the Global Positioning System.* PhD thesis, Stanford University, Department of Aeronautics and Astronautics, Stanford, CA 94305, March 1996.

[11] E. Harrison Teague, Jonathan P. How, London G. Lawson, Michael Boerjes, and Bradford W. Parkinson. Techniques for Real-Time Control of Flexible Structures Using GPS. In *Proceedings of the AAS Guidance and Control Conference*, Breckenridge CO, February 1996.

[12] E. Harrison Teague, Jonathan P. How, London G. Lawson, and Bradford W. Parkinson. GPS as a Structural Deformation Sensor. In *Proceedings of the AIAA Guidance, Navigation and Control Conference*, Baltimore MD, August 1995.

[13] K. R. Zimmerman and R. H. Cannon Jr. GPS-Based Control for Space Vehicle Rendezvous. In *Proceedings of the Institute of Navigation GPS-94 Conference*, Salt Lake City UT, September 1994.

APPENDIX

A General Differential Carrier Phase Analysis

The phase of an incoming, down-converted carrier wave may be written as (ignoring a constant offset)

$$\phi = (\omega - \omega_c)t + \frac{2\pi}{\lambda}x \tag{15}$$

where,

ω, λ - frequency and wavelength of incoming wave

Channel specific:

- ϕ - measured phase at the antenna phase center
- ω_c - downconverter reference oscillator frequency
- t - time of phase measurement applicability
- x - distance from the antenna to the transmitter

Fig. 9 shows a diagram of such a receiver channel. Let $\Delta(\cdot) = (\cdot)_2 - (\cdot)_1$. If we assume perfect phase lock in both receivers, and Δt small with respect to antenna motion bandwidth, the difference in carrier phase between two antennas is,

$$\Delta\phi = [(\omega - \omega_{c_2})t_2 - (\omega - \omega_{c_1})t_1] + \frac{2\pi}{\lambda}\Delta x \tag{16}$$

Neglecting second order terms, and letting $t_1 = t$ and $\omega_{c_1} = \omega_c$,

$$\Delta\phi = [(\omega - \omega_c)\Delta t - \Delta\omega_c t] + \frac{2\pi}{\lambda}\Delta x \tag{17}$$

The term in brackets represents error terms related to timing. Our receivers use antenna multiplexing and a

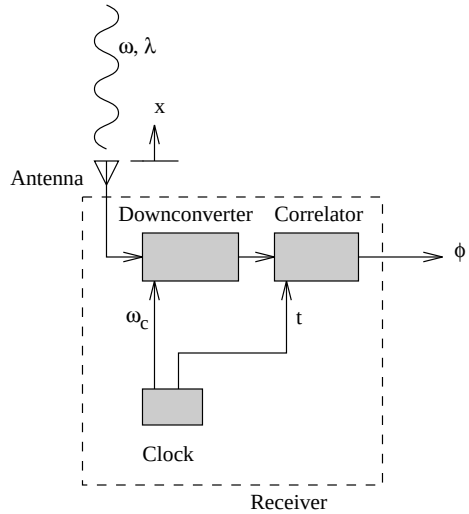

Figure 9: General Phase Reception Diagram

common clock reference, thus $\Delta\omega_c = 0$,

$$\Delta\phi = (\omega - \omega_c)\Delta t + \frac{2\pi}{\lambda}\Delta x \tag{18}$$

Now, Δt is a function only of multiplexing switching time and unequal antenna cable lengths. These are constant over time after phase lock, and thus constitute a line bias term.

In the absence of a common clock reference, other techniques must be employed to make use of the differential carrier observable, such as double differencing to remove relative clock offsets between differenced channels.

B Kinematic Estimator Observability Proof

<u>Theorem</u>: Given,

$$\tilde{H} = \left[\begin{array}{cccc|c} H^{(1)} & & & 0 & I \\ & H^{(2)} & & & I \\ & & \ddots & & \vdots \\ 0 & & & H^{(N)} & I \end{array}\right] \tag{19}$$

$\tilde{H}$ is not full column rank if any column of $H^{(i)}$ is constant for all i.

<u>Proof</u>: $\tilde{H}$ is not full column rank if all its columns are not linearly independent[6], equivalently, if we can find any $\tilde{v} \neq 0$ such that

$$\tilde{H}\tilde{v} = 0 \tag{20}$$

Let $h_k^{(i)}$ equal the kth column of $H^{(i)}$. Define v_k as a vector whose length equals the number of columns of

$H^{(i)}$, and whose elements are all zero except for the kth element, which is 1.

$$v_k = \begin{bmatrix} 0 \\ \vdots \\ 1 \\ \vdots \\ 0 \end{bmatrix} \leftarrow k_{th} \ element \tag{21}$$

Suppose,

$$\tilde{v} = \begin{bmatrix} v_k \\ v_k \\ \vdots \\ v_k \\ \hline v_I \end{bmatrix} \tag{22}$$

with v_I arbitrary. Then,

$$\begin{aligned} \tilde{H}\tilde{v} &= \begin{bmatrix} H^{(1)}v_k + v_I \\ H^{(2)}v_k + v_I \\ \vdots \\ H^{(N)}v_k + v_I \end{bmatrix} \\ &= \begin{bmatrix} h_k^{(1)} + v_I \\ h_k^{(2)} + v_I \\ \vdots \\ h_k^{(N)} + v_I \end{bmatrix} \end{aligned} \tag{23}$$

Thus, if $h_k^{(i)}$ is constant for all i, we can set the arbitrary $v_I = -h_k^{(i)}$, and then

$$\tilde{H}\tilde{v} = 0$$

DONE.